The organization of genome duplication is a critical determinant of the landscape of genome maintenance

Blanca Gomez-Escoda and Pei-Yun Jenny Wu

Genome Res. published online June 22, 2018
Access the most recent version at doi:10.1101/gr.224527.117

The organization of genome duplication is a critical determinant of the landscape of genome maintenance

Blanca Gómez-Escoda and Pei-Yun Jenny Wu*

Genome Duplication and Maintenance Team, Institute of Genetics and Development of Rennes, CNRS UMR 6290, 2 avenue du Pr. Léon Bernard, 35043 Rennes, France

**Corresponding author: Pei-Yun Jenny Wu; email: pei-yun.wu@univ-rennes1.fr, phone: +33 2 23 23 44 06*

Running title: Replication program and genome maintenance

Keywords: DNA replication, genome maintenance, fission yeast, replication stress, replication program

Abstract

Genome duplication is essential for cell proliferation, and the mechanisms regulating its execution are highly conserved. These processes give rise to a spatiotemporal organization of replication initiation across the genome, referred to as the replication program. Despite the identification of such programs in diverse eukaryotic organisms, their biological importance for cellular physiology remains largely unexplored. We address this fundamental question in the context of genome maintenance, taking advantage of the inappropriate origin firing that occurs when fission yeast cells lacking the ATR/Rad3 checkpoint kinase are subjected to replication stress. Using this model, we demonstrate that the replication program quantitatively dictates the extent of origin deregulation and the clustered localization of these events. Furthermore, our results uncover an accumulation of abnormal levels of single-stranded DNA (ssDNA) and the Rad52 repair protein at deregulated origins. We show that these loci constitute a defining source of the overall ssDNA and Rad52 hotspots in the genome, generating a signature pattern of instability along the chromosomes. We then induce a genome-wide reprogramming of origin usage and evaluate its consequences in our experimental system. This leads to a complete redistribution of the sites of both inappropriate initiation and associated Rad52 recruitment. We therefore conclude that the organization of genome duplication governs the checkpoint control of origin-associated hotspots of instability and plays an integral role in shaping the landscape of genome maintenance.

Introduction

Genome duplication is highly regulated to promote the faithful transmission of the genetic material during cell proliferation. In eukaryotes, DNA synthesis requires the coordinated assembly of conserved factors at the sites of replication initiation, or origins, distributed throughout the genome. Origins are licensed through the formation of the pre-replicative complex (pre-RC), which is followed by the assembly of the pre-initiation complex (pre-IC) that activates them for replication (Fragkos et al. 2015). This multistep process ensures that the genetic material is entirely copied once and only once during each cell cycle. Different initiation sites in a genome possess reproducibly distinct characteristics of usage: at the population level, each origin is activated with a particular frequency, or efficiency, and individual origins fire at given times during S phase (Heichinger et al. 2006). Moreover, a large body of work has characterized the presence of spatial and temporal patterns of replication, in which distinct genomic regions duplicate with particular timings during S phase, in diverse organisms (Hiratani et al. 2008; McCune et al. 2008; Muller and Nieduszynski 2012; Rhind and Gilbert 2013; Rivera-Mulia and Gilbert 2016). Collectively, the efficiencies, timings of firing, and positions of all of the origins in a genome define the program, or organization, of DNA replication.

The replication program has been shown to be highly flexible, and signature profiles have been established for diverse cell types and physiological states. For example, conserved replication timing domains have been identified in different human embryonic stem cell (ESC) lines, suggesting that they are a shared feature of pluripotence (Ryba et al. 2010). The differentiation of both mouse and human ESCs is then accompanied by alterations in the timing of duplication of large portions of the genome (Hiratani et al. 2008; 2010). The profile of origin usage is also sensitive to external stimuli, as seen in fission yeast cells that show changes in replication initiation after undergoing temporary nitrogen depletion (Wu and Nurse 2014). However, despite these observations, the biological importance of the replication program remains unclear. In particular, although the genome is particularly fragile when it is being copied (Aguilera and García-Muse 2013; Zeman and Cimprich 2014), little is known about whether and how the organization of DNA replication along the chromosomes may contribute to genome integrity. Potential evidence for such an interplay derives from genetic analyses that have correlated mutation frequency with replication timing on

chromosome VI in budding yeast (Lang and Murray 2011). In addition, whole-genome sequencing of normal and cancerous human cells has shown that late-replicating chromosomal regions often harbor point mutations and copy number losses, while copy number increases and other rearrangements occur more frequently in early-replicating domains (Koren et al. 2012; Liu et al. 2013). Finally, similar approaches have suggested a relationship between replication timing and differences in mutation rates across the genome in human cells (Stamatoyannopoulos et al. 2009; Chen et al. 2010). All together, these findings indicate that the replication program may be intimately coupled to genome maintenance.

The processes that preserve genome integrity are particularly essential when cells are under replication stress, as challenges to DNA synthesis can lead to the generation of lesions and errors. The S phase/ATR checkpoint response to such stress conditions comprises distinct functions, including transcriptional regulation, cell cycle arrest, stabilization of stalled replication forks, and inhibition of replication initiation at a subset of origins (Shirahige et al. 1998; Santocanale and Diffley 1998; Labib and De Piccoli 2011). While the importance of many of these mechanisms is well-described, this is not the case for the regulation of origin firing, despite a large body of work that has characterized the molecular players involved and initiation sites that are sensitive to checkpoint control (Feng et al. 2006; Heichinger et al. 2006; Hayashi et al. 2007; Mickle et al. 2007; Zegerman and Diffley 2010; Lopez-Mosqueda et al. 2010; Karnani and Dutta 2011; Poli et al. 2012). Indeed, it remains unknown how the origins that are targeted for inhibition in this context are selected, the extent to which inappropriate initiation occurs when the checkpoint is defective, and the consequences of deregulated replication initiation. In fact, the impact of this mechanism is still contested: for instance, using *SLD3* and *DBF4* budding yeast mutants that allow the firing of checkpoint-inhibited origins in replication stress conditions, Zegerman *et al.* found no effect on viability following exposure to the alkylating agent methyl methanesulfonate (MMS) (Zegerman and Diffley 2010); however, Lopez-Mosqueda and colleagues showed via the same approach that there is a 50% loss of viability upon nucleotide depletion by hydroxyurea (HU) treatment (Lopez-Mosqueda et al. 2010). These observations thus gave rise to contrasting views on the importance of the control of origin firing for the cellular response to replication stress. Nevertheless, the conservation of this regulation from yeast to humans strongly suggests that it is an integral feature of the processes that promote genome stability (Dimitrova and Gilbert 2000; Syljuåsen et al. 2005; Ge and Blow 2010; Karnani and Dutta 2011).

In this study, we have investigated the fundamental interplay between the program of DNA replication and genome maintenance, exploiting the checkpoint regulation of origin firing in fission yeast cells exposed to replication stress as a model. Our findings lead us to propose that the organization of genome duplication governs the checkpoint control of origin-associated hotspots of genome instability and shapes the landscape of genome integrity.

Results

Regional deregulation of origin firing in checkpoint-defective cells exposed to replication stress

As a model for our studies, we used the checkpoint control of origin firing in replication stress conditions, which provided us with a unique entry into the potential links between the organization of DNA replication and genome maintenance. To establish our system, we first addressed previous contrasting findings regarding this regulation in the fission yeast (Feng et al. 2006; Heichinger et al. 2006; Hayashi et al. 2007; Mickle et al. 2007). Indeed, various methods have identified significantly different subsets of checkpoint-regulated initiation sites, with 2% to 28% of the origins in the genome proposed to be sensitive to inhibition. One common feature of these studies is the use of high concentrations of the ribonucleotide reductase inhibitor HU (10-15 mM) to deplete nucleotide pools, and we hypothesized that this may have hindered the accurate detection of checkpoint-inhibited sites and contributed to the differences between these earlier reports. Furthermore, a quantitative assessment of the alterations in origin firing that are induced by replication stress in the absence of the checkpoint was lacking. We therefore began by characterizing the programs of origin usage in wild-type and checkpoint-defective *ATR/rad3Δ* fission yeast cells that replicate their DNA in the presence of moderate levels of HU (6 mM). Cells were synchronized in G2 using the *cdc25-22* temperature sensitive mutation and allowed to undergo S phase in HU (Supplemental Fig. S1A, see Methods). Genomic DNA samples were collected 5 min after the release from G2 (unreplicated DNA) and after a time when cells would normally have completed S phase in the absence of HU (replicated DNA, Supplemental Fig. S1B). Replication origins were then mapped using microarrays as previously described (Wu and Nurse 2014), and peaks of increased copy number in the replicating DNA samples were identified as initiation sites. Copy number was then converted to efficiency, which represents the frequency of firing of

a given origin in a population of cells (see Methods; details and validation of our copy number analyses are provided in the Supplemental Materials). In the context of our experiments, the major contribution to "efficiency" is replication initiation; however, our measurements do not exclude a minor contribution from passive replication. Nevertheless, the comparable widths of origin peaks between wild-type and *rad3Δ* cells indicate that origins are similarly affected by this potential input between the two genetic backgrounds. For simplicity, we will continue to refer to "% efficiency" to describe origin behavior.

Our data demonstrate substantial differences in replication initiation between wild-type and *rad3Δ* cells in replication stress conditions (Fig. 1A and Supplemental Fig. S1C; we will refer to the *cdc25-22* background without any other mutations as wild-type). While the usage of a majority of origins was unaltered, a number of sites were markedly increased in their efficiencies in checkpoint-defective cells. Applying a cutoff of 8% absolute difference in efficiency between wild type and *rad3Δ* (see Supplemental Methods for threshold selection), we identified 176 deregulated sites out of 876 total origins, with increases of up to 25% efficiency (Fig. 1B and Supplemental Tables S1 and S2). These inappropriate initiation sites are clearly distinguishable peaks and do not arise as a result of passive replication from neighboring origins (Supplemental Fig. S1C). Given that the average origin efficiency across the genome in wild-type cells is 29.3% and reaches a maximum of 66%, these alterations represent major changes in origin usage. We will refer to these deregulated origins as *C*heckpoint-*I*nhibited *O*rigins, or CIOs.

Next, we evaluated the characteristics and distribution of CIOs. CIOs span a broad spectrum of origin activities (Fig. 1B), contrasting with previous reports that only late-firing and inefficient origins in the genome are subject to checkpoint inhibition (Shirahige et al. 1998; Santocanale and Diffley 1998). Indeed, many inefficient sites showed no changes in usage, while origins with efficiencies up to 40% in wild-type cells were found to be deregulated (Fig. 1B). In fact, 30% of CIOs are among the first half of the origins that fire during S phase (Supplemental Fig. S1D), consistent with the known relationship between the timing and efficiency of origin firing (Heichinger et al. 2006; Wu and Nurse 2009). Notably, we observed that CIOs are clustered in distinct chromosomal regions (Fig. 1C, top panel), and we assessed what might underlie this distribution. To this end, we first ascertained the average efficiencies and timings of origin firing in a wild-type background in continuous 1000-probe (~250 kb) windows (Fig. 1C, bottom panel), which showed that

these two parameters are organized in virtually identical domains along the chromosomes. We then determined the percentages of origins that are deregulated in the same windows (Fig. 1C, middle panel). Our findings uncover a strong inverse relationship between the program of origin usage and inappropriate initiation at a regional level. Thus, our results demonstrate that 1) regardless of their individual efficiencies, CIOs are enriched in late-firing and inefficient regions of the genome, 2) a major fraction of the origins in these regions (up to ~70%) are deregulated in HU-treated *rad3Δ* cells, and 3) there are only a few CIOs outside of these regions, even in areas that contain some inefficient and late-firing origins. This distribution of CIOs is not biased by our specific experimental conditions, as we obtained similar results using a completely different method of synchronization (Supplemental Figs. S1A and S1F-G). Our results therefore provide a quantitative characterization of deregulated initiation and reveal a distinctive profile of checkpoint-inhibition of origin firing along the chromosomes that is linked to the replication program.

Finally, given the close link between the timing and efficiency of origin usage mentioned above (Heichinger et al. 2006; Wu and Nurse 2009), we asked if the increased initiation at CIOs is accompanied by earlier firing in S phase. For this analysis, we performed time courses of chromatin immunoprecipitation (ChIP) of the pre-IC component Cdc45 in cells undergoing a synchronous S phase in the absence or presence of HU after release from G2 arrest. We compared an early-firing and efficient origin whose activity is unaffected in HU-treated *rad3Δ* cells (*ori2004; oriBGE2105* in our study) with a late-replicating and inefficient CIO (*ori2060; oriBGE2122* in our study) (see Fig. 1D legend for efficiencies). In the absence of HU, *rad3Δ* did not affect the timing of firing of these origins (Fig. 1D). Moreover, while we observed a higher level of Cdc45 recruitment at *ori2060* exclusively in HU-treated *rad3Δ* cells, the timing of Cdc45 binding at *ori2060* was comparable between wild-type and *rad3Δ* cells. This indicates that the increased firing of CIOs is not accompanied by an early activation, consistent with previous work in budding yeast suggesting that the checkpoint does not regulate the temporal pattern of replication (Alvino et al. 2007).

Collectively, our findings demonstrate that in replication stress conditions, the ATR/Rad3 checkpoint inhibits origin firing based on the timing and efficiency of distinct genomic regions rather than the activity of individual origins. The unique distribution of deregulated replication initiation in checkpoint-defective cells subjected to nucleotide depletion, together with our extensive and quantitative assessment of these events,

makes this an ideal system for investigating whether the organization of genome duplication impacts genome maintenance.

Deregulation of origin firing locally induces the aberrant accumulation of single-stranded DNA

During DNA synthesis, single-stranded DNA (ssDNA) is transiently generated upon origin unwinding. In replication stress conditions, higher levels of ssDNA are produced, in particular when the checkpoint is compromised (Shechter et al. 2004; Feng et al. 2006). This represents a precursor to DNA damage (Feng et al. 2011), and we hypothesized that deregulated replication initiation may strongly contribute to generating such vulnerable sites. We therefore assessed the accumulation of ssDNA in wild-type and *rad3Δ* cells exposed to replication stress, taking advantage of the ssDNA binding protein Ssb1/RPA as a marker (Wold 1997). For these experiments, cells were synchronized in G2 and released to undergo S phase in the presence or absence of 6 mM HU. RPA binding was monitored by ChIP, comparing the unaffected efficient origin *ori2004* with *ori2060*, an inefficient CIO. At *ori2004*, we observed similar levels of RPA binding in both genetic backgrounds, either with or without HU exposure (Supplemental Fig. S2A). In contrast, we found a substantial increase in ssDNA at *ori2060* only in HU-treated *rad3Δ* cells: this did not occur either in wild-type cells or when HU was not applied. Furthermore, this effect was not simply due to the increase in initiation at *ori2060*: while *ori2004* has an efficiency of 50% and *ori2060* is at 26% in *rad3Δ* cells in HU, the level of RPA at *ori2060* was more than 3-fold higher than at *ori2004*. These data thus suggest that not all origins accumulate higher levels of ssDNA in *rad3Δ* cells in stress conditions and point to a specific dysfunction at deregulated origins.

We then determined the contribution of inappropriate origin firing to ssDNA formation genome-wide. We performed ChIP of RPA followed by microarray analysis (ChIP-chip) for wild-type and *rad3Δ* cells synchronized in G2 and released into 6 mM HU. Samples were collected early in S phase (60 min) and at a time in late S phase when we observed high RPA binding at *ori2060* (80 min) (Supplemental Figs. S1B and S2A). We note that replication has already initiated at a number of origins at 60 min (for simplicity and by comparison with the 80 min sample, we will refer to this time point as “early S”), as indicated by RPA binding (Figs. 2A-C and Supplemental Fig. S2B) and flow cytometry (Supplemental Fig. S1B). Our results

showed that in early S, wild-type and *rad3Δ* cells possess very similar profiles of RPA binding along the chromosomes (Fig. 2A, Early S; Supplemental Fig. S2B). Consistent with the origin unwinding that is a part of the normal initiation process, we found a comparable enrichment of RPA at most origins that directly correlates with efficiencies in both backgrounds (Fig. 2B and Supplemental Figs. S2C-D; Early S). In late S, ssDNA levels at early-firing and efficient origins were reduced, as expected from the duplication of these sites (Fig. 2B, Late S; Supplemental Fig. S2B). Importantly, in HU-treated *rad3Δ* cells, RPA was recruited at high levels to a subset of origins with a wide range of efficiencies (Fig. 2B, Late S), revealing a problem in replication initiation at these loci.

To evaluate the potential link between ssDNA accumulation and inappropriate initiation, we clustered origins into unaffected sites vs. CIOs and compared RPA recruitment. In early S, RPA was bound at efficient origins, but only CIOs displayed an increase in RPA binding in *rad3Δ* compared to wild-type cells (Fig. 2C and Supplemental Fig. S2D, Early S). This suggests that there is excess ssDNA formation at early-firing CIOs even during early S phase. Next, in late S, RPA binding to unaffected origins in either wild-type or *rad3Δ* cells was low, while it aberrantly accumulated at CIOs exclusively in the absence of the checkpoint (Fig. 2C and Supplemental Fig. S2D, Late S). This marked increase in RPA recruitment was centered on CIOs in HU-treated *rad3Δ* cells (Fig. 2D). Finally, we ascertained the relationship between the level of ssDNA formation and the extent of origin deregulation. To this end, the full complement of 876 origins was divided into 12 equal groups based on their differences in efficiencies between *rad3Δ* vs. wild-type in HU, and the average changes in efficiency and RPA occupancy were assessed for each group. Our analyses revealed a strong correlation between the alterations in origin usage and in the level of RPA binding (Fig. 2E). Taken together, these results implicate inappropriate initiation as a cause of abnormal ssDNA formation at these sites.

Although our studies indicate that origin deregulation leads to increased RPA binding, ssDNA may also accumulate at other genomic sites in these conditions. We identified all loci of significant RPA recruitment in late S phase in both wild-type and *rad3Δ* cells treated with HU, applying a stringent cutoff that excludes the low levels of ssDNA that are produced as part of the normal replication process (see Methods). While we identified only 18 RPA sites in wild type, we found 153 peaks in *rad3Δ* cells, with

CIOs representing 67% of these hotspots (Supplemental Fig. S2G). In addition, we noticed that changes in origin usage even below our 8% cutoff for CIOs were associated with abnormal ssDNA formation (Supplemental Figs. S2E-F); lowering our threshold to 5% resulted in the association of 78% of all RPA hotspots with this expanded set of deregulated origins. Thus, inappropriate initiation in these conditions is responsible for most of the sites of ssDNA accumulation in the genome.

Our results demonstrate that abnormal ssDNA accumulation is not a common feature of all replication origins in checkpoint-defective cells in stress conditions but rather occurs at a subset of sites that undergoes deregulation. This generates the large majority of the hotspots of ssDNA, providing evidence that unscheduled initiation is a key source of genome instability.

Deregulated origins are hotspots of Rad52 recruitment

The link between origin deregulation and ssDNA accumulation led us to investigate the local consequences of these events. The Rad52 protein is important for the repair of DNA double-strand breaks and the restart of stalled replication forks (Benson et al. 1998; Symington 2002; Lambert et al. 2010; Ait Saada et al. 2017), and its recruitment is used as a marker for genome instability (Van Dyck et al. 1999; Lisby et al. 2001). We monitored Rad52 binding at representative origins by ChIP in wild-type and *rad3Δ* cells synchronized in G2 and allowed to undergo S phase in 6 mM HU. At the unaffected origin *ori2004*, we did not detect Rad52 in either genetic background, with or without replication stress (Supplemental Fig. S3A), throughout the time course. However, at the CIO *ori2060*, there was a clear increase in Rad52 recruitment specifically in *rad3Δ* cells treated with HU, demonstrating that deregulation at this site is associated with an aberrant Rad52 accumulation. We then extended this analysis genome-wide, mapping Rad52 binding by ChIP-chip in HU-treated wild-type and *rad3Δ* cells (Fig. 3A and Supplemental Fig. S3B). Our results revealed a strong recruitment of Rad52 in late S (90 min) only at CIOs in *rad3Δ* cells exposed to HU (Figs. 3B-C, +HU; Supplemental Figs. S3C-D). This binding was also detected at low levels earlier in S phase (60 min) at a subset of CIOs but not at unaffected origins (Supplemental Figs. S3C-D). Importantly, we demonstrated that the alterations in Rad52 binding are quantitatively correlated with the extent of origin deregulation between *rad3Δ* and wild type (Fig. 3D, Supplemental Fig. S3E). This is consistent with the

direct correspondence between RPA and Rad52 levels at origins in late S phase (Supplementary Fig. S3F). In addition, an increase in Rad52 recruitment is observed at a small number of deregulated origins that did not meet our CIO cutoff (Supplemental Fig. S3E), suggesting that even low levels of unscheduled origin activation may have consequences for genome maintenance. Complementary to these analyses, we also ascertained the contribution of deregulated origin firing to overall Rad52 accumulation in HU-treated *rad3Δ* cells. To this end, we selected all the sites of significant Rad52 binding (see Methods), identifying 64 and 435 loci in wild type and *rad3Δ*, respectively. In *rad3Δ* cells, we found that 70% of CIOs are associated with Rad52 recruitment (Supplemental Fig. S3H) and that CIOs represent 31% of all Rad52 binding sites, constituting a key source of genome instability hotspots in these conditions. Moreover, we noted that the Rad52 levels associated with CIOs are higher than those co-localizing with unaffected origins or non-origin sites, indicating that CIOs are more likely to be problematic (Fig. 3E). All together, our results establish inappropriate initiation as a direct and major contributor to DNA damage.

Our finding that deregulated origins are hotspots of genome instability in HU-treated *rad3Δ* cells led us to ask whether they may already recruit Rad52 during an unperturbed S phase. To address this question, we performed ChIP-chip of Rad52 in wild-type and *rad3Δ* cells as above, synchronizing cells in G2 and allowing them to duplicate their DNA in the absence of HU. Rad52 recruitment was assessed 90 min after the release from G2, at the same time point as the late S experiments above. In these conditions, we observed similar genome-wide profiles of Rad52 binding in wild-type and *rad3Δ* cells (Supplemental Fig. S3G, bottom panels). However, they differed significantly from the pattern in checkpoint-defective cells exposed to replication stress (Supplemental Fig. S3G, top panels). Heat map and quantitative analyses demonstrated that the distinctive accumulation of Rad52 at CIOs in HU-treated *rad3Δ* cells is not observed in an unperturbed S phase (Figs. 3B-C, -HU). For instance, in *rad3Δ* cells, only 5% of CIOs are associated with Rad52 peaks in the absence of HU, while 70% of CIOs recruit Rad52 upon HU exposure (Supplemental Fig. S3H). This suggests that CIOs are not particularly problematic in a normal S phase and uncovers a pivotal role for the checkpoint in regulating origin firing to preserve genome stability when cells are subjected to replication stress.

Origin selection in replication stress conditions delineates the profile of genome instability

We have shown that CIO deregulation in nucleotide-depleted *rad3Δ* cells gives rise to problematic sites that recruit the DNA repair machinery. However, genome instability in replication stress conditions arises from a variety of sources (Aguilera and García-Muse 2013; Zhou et al. 2013; Hoffman et al. 2015), and a significant portion (38%) of the Rad52 peaks in *rad3Δ* cells is not associated with origins (Supplemental Fig. S3H). We therefore evaluated the relationship between the genome-wide landscape of instability and inappropriate replication initiation, taking into account all 876 origins as well as all RPA and Rad52 binding sites in HU-treated cells. Regional analyses over continuous 1000-probe (~250 kb) windows revealed a clear correspondence between origin deregulation vs. the densities of RPA and Rad52 loci in a *rad3Δ* mutant (Fig. 4A). Furthermore, the signature Rad52 profile of HU-treated *rad3Δ* cells was not observed in situations where origins are not deregulated, either in 1) HU-treated wild-type cells or 2) during a normal S phase in both wild-type and *rad3Δ* backgrounds (Supplemental Fig. S4). These results establish unscheduled origin firing as a critical determinant of the overall pattern of genome instability. Finally, as suggested by these data and by the clustering of CIOs in late-firing and inefficient domains (Fig. 1C), we found that origin deregulation and Rad52 binding in *rad3Δ* cells under replication stress show strong negative correlations with the wild-type program of origin efficiencies (Fig. 4B). Collectively, our results allow us to propose a model in which the organization of DNA replication delimits the checkpoint regulation of origin firing in cells exposed to replication stress, with key consequences for the landscape of DNA damage in checkpoint-compromised cells.

Impact of altering the program of genome duplication on origin deregulation

While our studies suggest that the replication program regulates the inhibition of origin usage by ATR/Rad3, they do not exclude the possibility that the checkpoint may simply be more readily recruited to particular chromosomal regions that may be fragile or susceptible to insults (Aguilera and García-Muse 2013). To distinguish between these possibilities, we used a *rif1Δ* genetic background, in which replication initiation is altered genome-wide. Rif1 is a determinant of replication timing, and the differences in the timing of firing of early vs. late origins are reduced in *rif1Δ* mutants (Hayano et al. 2012; Cornacchia et al.

2012; Yamazaki et al. 2012; Foti et al. 2016). Relevant to our studies, loss of Rif1 function in the fission yeast does not alter sensitivity to replication stress (Hayano et al. 2012). First, we evaluated the effect of *rif1Δ* in our experimental setup and determined origin usage in *cdc25-22 rif1Δ* cells synchronized in G2 and released in 6 mM HU (Supplemental Fig. S5A). Consistent with previous reports, we observed major changes in the replication program compared to that in wild type (Supplemental Fig. S5B). We then assessed the regional profile of DNA replication by ascertaining average origin efficiencies in continuous 1000-probe windows as for Fig. 1C and found that the characteristic differences between efficiency domains in wild-type cells are strongly attenuated in *rif1Δ* (Fig. 5A). This background thus represents an ideal system for testing our model: if the replication program delimits the regions where the checkpoint inhibits origin firing in replication stress conditions, we would predict that inappropriate replication initiation in a *rif1Δ rad3Δ* mutant would no longer be enriched in the same genomic domains as in *rad3Δ*.

We therefore analyzed the impact of the altered replication program in *rif1Δ* cells on origin deregulation, comparing efficiencies in *rif1Δ rad3Δ* and *rif1Δ* cells arrested in G2 and allowed to synchronously enter S phase in 6 mM HU (Fig. 5B and Supplemental Fig. S5C). Applying the same 8% threshold as for CIOs, we identified 170 deregulated origins in *rif1Δ rad3Δ* cells that we will refer to as *rif1*-CIOs (Fig. 5B, Supplemental Tables S4-S5). These *rif1*-CIOs also span a broad spectrum of activities (Supplemental Fig. S5D). However, in contrast to CIOs, *rif1*-CIOs are more uniformly positioned along the chromosomes and no longer clustered in distinct domains (Fig. 5C and Supplemental Fig. S5C); this reflects the "flattened" replication profile in *rif1Δ*. Notably, a large number of *rif1*-CIOs are found in regions that lack CIOs in *rad3Δ*. These findings demonstrate that inappropriate origin activation does not occur as a result of the chromosomal context but rather as a consequence of the program of DNA replication.

Changes in origin deregulation redistribute hotspots of Rad52 recruitment

We next determined whether the changes in origin deregulation in checkpoint-deficient *rif1Δ* cells treated with HU are accompanied by a redistribution in Rad52 recruitment. To this end, *rif1Δ* and *rif1Δ rad3Δ* cells were allowed to synchronously enter S phase in 6 mM HU, and Rad52 binding was assessed by ChIP-chip 90 min after the release, when we observed high levels of Rad52 recruitment at a representative

rif1-CIO (Supplemental Fig. S6A). First, our results in *rif1Δ* cells showed that this mutation itself does not induce either high levels of Rad52 binding compared to wild type (Supplemental Fig. S6B) or Rad52 recruitment at origins (Supplemental Fig. S6C). Importantly, we found a genome-wide increase in Rad52 binding in HU-treated *rif1Δ rad3Δ* cells compared to *rif1Δ* (Fig. 6A, Supplemental Fig. S6D). Heat map analyses revealed a clear enrichment of Rad52 at a number of origins in *rif1Δ rad3Δ* that was not detected in *rif1Δ* (Fig. 6B, +HU). Although our 8% efficiency cutoff identified only a subset of these sites as *rif1*-CIOs, we established a clear positive correlation between the increases in origin efficiencies in *rif1Δ rad3Δ* and the changes in Rad52 binding (Fig. 6C), indicating higher levels of recruitment at *rif1*-CIOs. Building on these findings, we then determined the extent to which inappropriate initiation contributes to Rad52 hotspots in these cells. Using the same criteria as for our previous analyses (Supplemental Fig. S3H), we identified 618 sites of Rad52 binding in HU-treated *rif1Δ rad3Δ* cells compared to 94 in *rif1Δ*. Similar to our observations for CIOs in *rad3Δ*, 62% of the 170 *rif1*-CIOs coincide with Rad52 hotspots in *rif1Δ rad3Δ*, and 67% of all Rad52 loci are in fact associated with origins (Supplemental Fig. S6E). Together with Fig. 6C, which exposes a strong correlation between origin deregulation and Rad52 accumulation even for origins that were not initially identified as *rif1*-CIOs, these results indicate that inappropriate initiation is a major source of genome instability hotspots in *rif1Δ rad3Δ* cells exposed to replication stress.

Given the large number of Rad52 binding sites in HU-treated *rif1Δ rad3Δ* cells, we addressed the possibility that the altered origin usage program in a *rif1Δ* background generates a sensitized state in which cells experience replication stress even during an unperturbed S phase. To this end, we ascertained Rad52 binding in synchronized *rif1Δ* and *rif1Δ rad3Δ* cells that proceeded through S phase in the absence of HU, taking the same time point (90 min) as for Fig. 6A. Heat map analyses of data from both strains showed that in these conditions, Rad52 is not enriched at either unaffected origins or *rif1*-CIOs (Fig. 6B, -HU). Indeed, in contrast to HU-treated *rif1Δ rad3Δ* cells, where 62% of *rif1*-CIOs overlap with Rad52 sites, only 10% of *rif1*-CIOs coincide with Rad52 loci in a normal S phase (Supplemental Fig. S6E). These data therefore suggest that the altered replication program in *rif1Δ* is not intrinsically problematic and that absence of the checkpoint in this context does not give rise to origin-associated DNA damage.

Finally, we evaluated the overall impact of reprogramming DNA replication on the landscape of genome instability. We compared the density of Rad52 hotspots over continuous 1000-probe windows in *rif1Δ rad3Δ* and *rad3Δ* cells in the absence and presence of HU. In an unperturbed S phase, this pattern was highly similar between the two strains (Fig. 6D, bottom panel), implying that the *rif1Δ* mutation itself does not induce a significant alteration of the Rad52 profile in a sensitized, checkpoint-defective background. In replication stress conditions, Rad52 sites in *rif1Δ rad3Δ* cells were no longer clustered in the same distinct genomic domains as in *rad3Δ* (Fig. 6D, top panel), revealing a complete redistribution of Rad52 loci.

Taken together, these findings support our model that induced alteration of the replication program in checkpoint-defective cells subjected to replication stress leads to changes in the pattern of deregulated replication initiation as well as associated genome instability events.

Discussion

In this study, we have identified a fundamental role for the program of genome duplication in the maintenance of genome stability. Our results demonstrate that in checkpoint-defective cells subjected to replication stress, the significant deregulation of ATR/Rad3-inhibited origins is clustered in late-replicating and inefficient genomic domains. We show that this selective regulation of origin usage by the checkpoint is directly and quantitatively governed by the program of genome duplication, regardless of the individual characteristics of these origins. We observe a strong correlation between the extent of origin deregulation and the levels of RPA and Rad52 binding at these loci. These inappropriate origin firing events represent a major source of the genome-wide complement of Rad52 hotspots, and the distinctive localization of these sites delineates a signature profile of genome instability. Finally, modulation of the replication program using a *rif1Δ* mutant background leads to an entirely altered pattern of origin deregulation in checkpoint-defective cells subjected to replication stress. In this context, the link between unscheduled initiation and Rad52 accumulation is nevertheless maintained, which results in a genome-wide redistribution of problematic loci. Our work therefore provides novel evidence that the organization of DNA replication establishes the landscape of checkpoint-regulated origin firing and shapes genome instability along the chromosomes.

The results of our study have critical implications for the cellular response to genotoxic insults. While previous investigations focused on the targeting of late-firing and inefficient origins, with work in budding yeast showing that such sites are not fired when the checkpoint is functional (Poli et al. 2012), our data reveal that individual origins with a broad range of efficiencies and firing times are in fact subject to checkpoint inhibition. Our findings are compatible with an earlier study in which origins repressed by the checkpoint in HU eventually fire after a long period of time, hinting that the checkpoint does not specifically control a distinct set of late-firing origins (Alvino et al. 2007). In particular, we establish that in nucleotide-depleted *ATR*/*rad3* mutants, the number of deregulated origins in a region and the changes in their efficiencies are directly coupled to the characteristics of replication efficiency and timing domains. In addition, in the context of the stochasticity in replication initiation observed in DNA combing assays (Patel et al. 2006; Czajkowsky et al. 2008; Kaykov and Nurse 2015), we do not interpret our results to imply that

every origin in late-replicating domains is deregulated in each cell, but rather that there is a higher frequency of inappropriate initiation in these regions. Our data reveal that the control of origin usage by the ATR/Rad3 pathway in replication stress conditions is a key aspect of its function in genome maintenance. Our work also presents compelling evidence for a fundamental biological importance of the replication program in genome surveillance, which may help to elucidate the rationale for the pattern of DNA replication in wild-type cells. For example, particular programs may lead to elevated local concentrations of checkpoint factors that would protect at-risk regions through more efficient signaling (Rivera-Mulia et al. 2015). This may favor the repression of neighboring sites and also locally enhance DNA repair processes. Complementary to this, there may also have been evolutionary selection for an arrangement in which potential sites of DNA damage are enriched in regions where mutations have a lower likelihood to be deleterious.

Although we have focused on the regulation of replication initiation in stress conditions, our findings may also be applicable to an S phase that is not subjected to pathological replication stress. Indeed, cells can encounter multiple challenges to DNA synthesis even in "unperturbed" conditions (Zeman and Cimprich 2014). For instance, markers of genotoxic stress are detected during replication in embryonic stem cells (Ahuja et al. 2016), and ATR function is essential in other eukaryotic systems (Eykelenboom et al. 2013). In addition, replication stress may be induced by the dependence of DNA synthesis on limiting factors that include components of the replication machinery (Cdc45, Sld2, and Sld3) (Wu and Nurse 2009; Mantiero et al. 2011; Tanaka et al. 2011) as well as those that are critical for efficient replication, such as RPA (Toledo et al. 2013). dNTPs are also limiting during genome duplication: the existing pool of dNTPs at G1/S is insufficient to complete replication, and the ribonucleotide reductase (RNR) is induced to produce the necessary nucleotides (Poli et al. 2012; Guarino et al. 2014). However, while there are multiple potential sources of challenges to replication during a normal S phase, we do not find Rad52 recruitment to origins in the absence of HU treatment in our experimental context. Nevertheless, it is possible that in this situation, cells experience only mild intrinsic levels of stress, making inappropriate initiation events relatively rare and difficult to monitor using our short-term population-level analyses. Indeed, there are indications that the organization of DNA replication may have long-term consequences for genome architecture and maintenance. For instance, our demonstration that origins are hotspots of genome instability when inappropriately fired in stress conditions is consistent with comparative genomic analyses and laboratory

evolution experiments in budding yeast that have co-localized breakpoints for gene amplifications and chromosome rearrangements with origins (Di Rienzi et al. 2009; Gordon et al. 2009). Our results also hint at a mechanism for how the replication program may delineate differences in the types and rates of mutations that have been associated with replication timing (Lang and Murray 2011; Liu et al. 2013). All together, these possibilities have important implications for the processes that shape the genome during its evolution.

Finally, our studies may bring insight into the mutations that accumulate when DNA synthesis is perturbed in pathological situations, such as in cancer. Early tumorigenesis is associated with replication stress and nucleotide deficiencies (Halazonetis et al. 2008; Bester et al. 2011), and a haploinsufficiency of ATR or Chk1 has been shown to contribute to cancer predisposition (Brown and Baltimore 2000; Lam et al. 2004). Furthermore, cancer cells have been found to display altered patterns of origin usage (Donley and Thayer 2013). Our experimental conditions therefore recapitulate many of these features, and our results suggest that the replication program may be responsible for the differential susceptibility of distinct genomic regions to the accumulation of DNA damage in these contexts. Our conclusions may thus inform the current understanding of how the cancer mutational landscape arises, with consequences for somatic evolution and for the heterogeneity found in individual tumors.

While our previous work coupled origin selection with programmed recombination in the context of the specialized meiotic cycle (Wu and Nurse 2014), our new findings demonstrate that the replication program has a broader and more fundamental role in cellular biology through regulating the surveillance pathways that ensure the fidelity of the genetic material. The conservation of the mechanisms for DNA replication and checkpoint regulation from yeast to humans suggest that this critical function of the organization of genome duplication in genome maintenance may also extend to more complex eukaryotic systems.

Methods

Strains and cell growth

Standard media and methods for fission yeast were used (Hayles and Nurse 1992; Moreno et al. 1991). Cells were grown in minimal medium supplemented with 250 mg/L adenine, histidine, lysine, uracil, leucine, and arginine (EMM6S). Supplemental Table S6 lists the fission yeast strains used in this study. The following constructions were previously generated: Cdc45-YFP (Gregan et al. 2003), *rad3Δ::ura4* (gift from the Nurse Lab), and Polδ-Flag (Taricani and Wang 2006). Deletions and tagged proteins (*rad3Δ::kanMX*, *rif1Δ::natMX,* Ssb1-HA) were constructed by homologous recombination (Bähler et al. 1998). The JW129 and JW131 strains were used for the origin mapping and ChIP-qPCR experiments in Fig. 1 and Supplemental Fig. S1. JW133 and JW135 were used for the Ssb1/RPA ChIP-chip experiments (Fig. 2 and Supplemental Fig. S2). PN292 and JW154 were used for the Rad52 ChIP-chip experiments (Fig. 3 and Supplemental Fig. S3). JW1183 and JW1184 were used for both the origin mapping and Rad52 ChIP-chip experiments in a *rif1Δ* background (Figs. 5-6 and Supplemental Figs. S5-S6). PN2483 and JW1135 were used for determination of origin efficiencies after synchronization with *nda3-km311* (Supplemental Fig. S1). PN1 and PN1400 were used for validation of copy number experiments (Supplemental Fig. S7).

Cell cycle synchronization

Strains with the *cdc25-22* mutation were grown at the permissive temperature (25 ºC) to a density of ~$2x10^6$ cells/mL before being shifted to the restrictive temperature (36.5 ºC) for 4 h, leading to G2 arrest (Forsburg and Rhind 2006). Subsequent release to 25 ºC by rapid cooling of the culture results in synchronous entry into mitosis and S phase. For *nda3-km311* strains, cells were grown in exponential phase at 32 ºC to a density of ~$2x10^6$ cells/mL and shifted to 18 ºC for 6 h to induce mitotic arrest (Hiraoka et al. 1984). Release to 32 ºC results in synchronous re-entry into the cell cycle.

Flow cytometry

Cells were fixed in 70% cold ethanol, washed in 50 mM sodium citrate and treated with RNase A (0.1 mg/mL) at 37 ºC. Samples were then stained using 2 mg/mL propidium iodide, sonicated with a Branson digital sonifier, and run on a BD Accuri C6 flow cytometer (BD Biosciences, USA). Data were analyzed using the FlowJo software. Details for the interpretation of flow cytometry profiles in the fission yeast are provided in the Supplemental Material section.

Chromatin immunoprecipitation

ChIP experiments were performed as previously described (Wu and Nurse 2009). Cells were fixed with 1% formaldehyde, lysed in a FastPrep cell disruptor (MP Biomedicals, USA) and sonicated with a Bioruptor Plus (Diagenode) to obtain chromatin fragments of ~400-500 bp. Immunoprecipitations (IP) were carried out overnight at 4 ºC using the following antibodies: α-GFP rabbit polyclonal antibody for Cdc45-YFP (gift from the Nurse Lab), α-Rad52 (Ab63800; Abcam, UK), and α-HA for Ssb1-HA (12CA5; Roche, Switzerland). Protein G sepharose beads (GE Healthcare, USA) were then added to the samples and incubated for 4 h at 4 °C. IPs were then washed and eluted, and crosslinking was reversed for both IP and Input samples by incubation at 65 ºC overnight. For quantitative PCR, IP and Input DNA were mixed with SYBR Green qPCR Master Mix (Agilent Technologies, USA) and processed with an ABI 7900 HT. Primers used in this study are listed in Supplemental Table S7.

Origin mapping experiments and analyses

Competitive hybridizations of differentially labeled samples were performed using Agilent 4x44k *S. pombe* arrays (60-mer probes every ~250 nucleotides; Agilent Technologies, USA) as previously described (Wu and Nurse 2014). Briefly, copy number was determined by comparing genomic DNA samples from non-replicating cells and from cells undergoing DNA replication in hydroxyurea (HU). HU treatment limits the extension of DNA synthesis around the sites of initiation, allowing the identification of replication origins. This method has been validated in previous studies (Heichinger et al. 2006; Wu and Nurse 2014) and

provides very similar origin maps to those obtained with other approaches (Daigaku et al. 2015; Hayashi et al. 2007). In *cdc25-22* experiments, 6 mM HU was added 5 min after cells were released from the G2 arrest; samples were taken at this time and after a time when cells would normally have completed S phase in the absence of HU (90 min). For *nda3-km311*, 6 mM HU was added 5 min after cells were released from mitotic arrest; samples were taken just before the release and 80 min after release.

Genomic DNA was extracted (Hoffman and Winston 1987) and purified using the Qiagen Genomic DNA kit. Samples were labeled using the BioPrime Plus Array CGH Indirect Genome Labeling Kit (Invitrogen, USA) according to manufacturer's instructions with either Alexa 555/647 (Agilent Technologies, USA) or Cy3/Cy5 (GE Healthcare, USA) dyes. 1-2 µg of labeled DNA from the unreplicated and S phase samples were hybridized onto the microarrays. Two independent hybridizations of the same samples were systematically performed in a dye-swap experiment, the ratios of replicating DNA to unreplicated DNA were assessed, and these datasets were averaged. To determine copy number, the geometric means over five consecutive probes were determined across the genome. Outliers were identified and removed prior to origin assignment. We averaged three biological repeats for *cdc25-22* vs. *cdc25-22 rad3Δ* as well as for *cdc25-22 rif1Δ* vs. *cdc25-22 rif1Δ rad3Δ*; two biological repeats were used for the *nda3-km311* vs. *nda3-km311 rad3Δ* comparison. To obtain origin efficiencies, the lowest ratios, which represent non-replicated DNA (a small proportion of the genome in 6 mM HU), were adjusted to be centered on a value of 1. This resulted in a correction of 0.25 for all datasets. The application of this correction was further validated by visual inspection of the overall profiles. Copy number was converted to efficiency (for example, 1.5 = 50%), which represents the frequency of firing of a given origin in a population of cells. Supplemental Tables S1-S5 provide information regarding origin positions and efficiencies in our experimental conditions. Additional details of our analyses of origin efficiencies and the selection of deregulated origins are provided in the Supplemental Methods and in Supplemental Figs. S7-S9.

ChIP-chip analysis

For ChIP-chip assays, 150 mL of cells were collected after release from G2 arrest at either 60 min or 80 min for Ssb1/RPA and at 60 min or 90 min for Rad52. ChIPs were performed as described above. For

amplification of the ChIP material and labeling for hybridization, the protocol from (van Bakel et al. 2008) was used according to (Wu and Nurse 2014). Each ChIP was then hybridized against its reciprocally labeled Input sample (IP/Input). For HU-treated *cdc25-22* and *cdc25-22 rad3Δ* cells, three biological repeats were performed for RPA and Rad52. Two biological repeats were performed for Rad52 in HU-treated *cdc25-22 rif1Δ* and *cdc25-22 rif1Δ rad3Δ*. For all Rad52 experiments in the absence of HU, two biological repeats were performed.

For all quantitative analyses (measurement of binding at origins, heatmaps, average signal plots, and selection of binding sites), probe values were used directly. For visual representation in Figs. 2A, 3A, and 6A as well as Supplemental Figs. S2B, S3B, S3G, S6A, and S6C, the moving geometric means of five consecutive probes were calculated across the genome and plotted.

To identify peaks of RPA or Rad52 recruitment, we designated a position as a binding site only when 3 consecutive probes showed values higher than our thresholds. For RPA, we established a cutoff of 2.0 based on the values of IP/Input for all the probes in a wild-type background after calculating the dispersion of the data from the median. Values were divided into quartiles, and as RPA only binds to specific sites, we considered that the median value of the dataset represents the unbound DNA and that significant binding occurs only when the values are 1.5 times the interquartile range (IQR) above the third quartile (Q3 + 1.5(IQR)=1.84). This cutoff excludes low levels of RPA that are part of the normal replication process. For Rad52, a threshold of 1.5 for IP/Input was established. This was based on the distribution of the signal IP/Input for all the probes in a wild-type background, after calculating the dispersion of the data from the median (Q3 + 1.5(IQR) = 1.48). We considered RPA and Rad52 sites to co-localize with an origin if they occurred within a distance of < 3 kb.

Quantitative and statistical analyses

For the quantitative analyses in Figs. 2D-E, 3C-D, and 6C as well as in Supplemental Figs. S2C-G, S3D-F, S4 and S6B, the levels of RPA and Rad52 recruitment were determined as follows: for each origin, we took the two probes closest to the origin position and identified the larger value for either RPA or Rad52

binding. This was then used as the occupancy at that origin. Statistics were performed with R Studio. The correlations in Fig. 4 and Supplemental Fig. S4 were tested using the Spearman's rank correlation coefficient. The correlations in Supplemental Fig. S9A were tested using the Pearson correlation coefficient.

The heat maps in Figs. 2B-C, 3B, 6B, and Supplemental Fig. S3C were generated using R Studio (RStudio Team 2015). Levels of RPA and Rad52 binding were converted to a log(2) scale. Origins were then aligned on a central position, and the log(2) values within a distance of -100 to +100 probes from this position were plotted. For visualization, log(2) values < 0.5 were assigned a value of 0. For the average signal plots in Figs. 2D and 3C, the means of the values were calculated for a distance from -100 to +100 probes centered on the origins.

Data access

All microarray data from this study have been submitted to the NCBI Gene Expression Omnibus (GEO; https://www.ncbi.nlm.nih.gov/geo/) under accession number GSE98462.

Acknowledgements

We thank members of the Genome Duplication and Maintenance team for helpful suggestions, in particular Anthony Perrot for experimental as well as bioinformatics assistance and Diane Schausi-Tiffoche for technical aid. We are grateful to Biogenouest Genomics and the Human Environmental Genomics core facility of Rennes (Biosit/OSUR) for technical support. We also thank Damien Coudreuse for valuable discussions and critical reading of the manuscript.

This study was supported by funding from Worldwide Cancer Research (11-0685), the CNRS/INSERM (ATIP-Avenir program), the Fondation pour la Recherche Médicale ("Amorcage de jeunes equipes" program), the Fondation ARC (Projet ARC), the *Ligue contre le cancer (Comités 22, 29, and 35)*, and the Institut National du Cancer (INCA, PLBIO 15-043). PYW was also supported by the Région Bretagne and Rennes Métropole. The funding bodies had no role in the design and progress of this study.

Author contributions

Conceived and designed the experiments, analyzed the data, wrote the paper: BGE and PYW. Performed the experiments: BGE. Supervised the study: PYW.

Disclosure declaration

The authors declare no competing interests.

Figure legends

Figure 1: Regional deregulation of origin firing in checkpoint-defective cells exposed to replication stress. A) Origin efficiencies in a representative region of the genome for *cdc25-22* (black, WT) and *cdc25-22 rad3Δ* (red, *rad3Δ*) cells in 6 mM HU (see Supplemental Figs. S1A-B for experimental design and flow cytometry analyses). Full profiles are shown in Supplemental Fig. S1C. Asterisks mark CIOs. x-axis: chromosome coordinates, y-axis: origin efficiency. **B)** Analysis of the absolute efficiency differences between *rad3Δ* and wild-type (WT) cells as a function of origin usage in WT (data from A and Supplementary Fig. S1C). x-axis: origin efficiency in WT, y-axis: differences in origin efficiency (*rad3Δ* - WT). Open circles: unaffected origins; red circles: CIOs (see Methods for CIO selection). Lines mark 8% differences in absolute origin efficiency. **C)** Clustering of deregulated origins in late-firing and inefficient chromosomal domains. Top: Red bars indicate positions of CIOs. Middle: Comparison of origin deregulation in *rad3Δ* with the program of replication in WT. The percentages of CIOs in 1000-probe (~250 kb) windows were determined across the genome (blue line, scale on left y-axis). The averages of origin efficiencies in WT were assessed for the same continuous windows (black line, scale on right y-axis). Bottom: The profiles of replication timing and efficiency in a wild-type (WT) background show identical regional characteristics. The average timings of origin firing were assessed for the same continuous windows as above (purple, left y-axis; timing data from Heichinger et al. 2006). The profile of efficiency domains is as in the middle panel (black, right y-axis). x-axis: chromosome coordinates. Note that regions containing CIO clusters are also enriched in sites of inappropriate origin firing that were identified in previous studies (Supplemental Fig. S1E). **D)** Time course of Cdc45 binding in *cdc25-22* (WT, black) and *cdc25-22 rad3Δ* (*rad3Δ*, red) cells at an unaffected origin (*ori2004*, closed circles) and a CIO (*ori2060*, open circles). Cells were released from G2 arrest and sampled at the indicated time points. In replication stress conditions, *ori2004* is used with an efficiency of ~50% in wild type and *rad3Δ*, while the efficiency of *ori2060* increases from 14% in wild type to 26% in *rad3Δ* (Supplemental Table S1). Top: -HU, bottom: 6 mM HU. x-axis: time after release, y-axis: Cdc45 occupancy (%IP).

Figure 2: Abnormal accumulation of ssDNA at deregulated origins. A) Profiles of RPA binding and origin usage in a representative region of the genome. Full RPA and origin profiles are in Supplemental Fig.

S2B. Top and middle: RPA recruitment in early (60 min, top) and late (80 min, middle) S phase in wild type (WT, gray) and *rad3Δ* (orange). y-axis: RPA binding (IP/input). Bottom: origin efficiencies for WT (black) and *rad3Δ* (red). Asterisks mark CIOs. y-axis: origin efficiency. x-axis for all panels: chromosome coordinates. **B)** Heat maps of RPA recruitment at origins in HU-treated wild-type (WT) and *rad3Δ* cells in early and late S phase. Data are from ChIP-chip experiments in A and Supplemental Fig. S2B. All origins are shown in order of increasing efficiency; the most efficient origins are at the bottom of the plot. Position 0: central probe for each origin; values in a window of 100 probes on either side of each origin are displayed. A more intense red represents a higher level of RPA binding. **C)** Heat maps of RPA recruitment, with origins divided into two categories: unaffected origins and CIOs (data are the same as in B). Origins in each category are displayed according to their efficiencies. Probe positions and color codes are as in B. **D)** Average signal plots of RPA binding at origins in HU. Each line represents average RPA binding at either unaffected origins (solid lines) or CIOs (dotted lines) in wild-type (WT, black) and *rad3Δ* (red) cells. Position 0: central probe for each origin; values at each probe position in a 100-probe window on either side of each origin were averaged for all origins in a category. **E)** Correlation between the differences in RPA binding and in origin usage between *rad3Δ* and wild-type (WT). Origins were divided into 12 equal subsets (73 origins/group) based on the changes in their efficiencies (*rad3Δ* – WT). The average differences in efficiency (x-axis) and RPA occupancy (y-axis) for each group are shown. The non-averaged data are shown in Supplemental Fig. S2E.

Figure 3: Rad52 is recruited to deregulated origins. A) Rad52 binding and origin usage in replication stress conditions. A representative region of the genome is shown. Full Rad52 profiles are in Supplemental Fig. S3B, full origin maps are in Supplemental Fig. S1C. Top: Rad52 recruitment in wild type (WT, gray) and *rad3Δ* (blue). y-axis: Rad52 binding (IP/input). Bottom: origin efficiencies for wild-type (WT, black) and *rad3Δ* (red). Asterisks mark CIOs. y-axis: origin efficiency. x-axis for top and bottom: chromosome coordinates. **B)** Heat maps of Rad52 binding at origins in HU-treated cells (left) or during an unperturbed S phase (right). Data are from ChIP-chip experiments as in A and Supplemental Fig. S3G. Data analysis and presentation are as in Fig. 2C. Note that there are a few red horizontal lines in *rad3Δ* in –HU: these represent high levels of Rad52 recruitment to the end of the right arm of chromosome III (Supplemental Fig. S3B), which we have not further investigated in this study. **C)** Average signal plots of Rad52 binding at origins in

HU-treated cells (top) or during an unperturbed S phase (bottom). Data analysis and presentation are as in Fig. 2D. Black: wild-type (WT), red: *rad3Δ*. Solid lines: unaffected origins, dotted lines: CIOs. **D)** Correlation between the differences in Rad52 binding and in origin usage between *rad3Δ* and wild-type (WT). Data analysis and presentation are as in Fig. 2E. x-axis: difference in origin efficiency, y-axis: difference in Rad52 binding. The non-averaged data are shown in Supplemental Fig. S3E. **E)** Levels of Rad52 binding at peaks associated with unaffected origins, CIOs, and non-origin sites. Each point represents a single origin. Red lines: median values for each category of Rad52 peaks. x-axis: level of Rad52 binding (IP/input).

Figure 4: The profile of origin deregulation delineates the profiles of RPA and Rad52 binding in replication stress. A) Genome-wide comparisons of origin deregulation and genome instability. This analysis takes into account all 876 identified origins as well as all RPA and Rad52 binding sites. The sum of the changes in origin efficiencies upon HU treatment (*rad3Δ* - WT, red) was determined in continuous 1000-probe windows. The densities of RPA (orange) and Rad52 (blue) sites were calculated for HU-treated *rad3Δ* cells over the same windows. x-axis: chromosome coordinates; y-axes: sum of the differences in origin efficiencies (top), density of RPA sites (middle), density of Rad52 sites (bottom). The Spearman's correlation coefficients (ρ) for the different comparisons are indicated and show strong positive correlations. ***: p-value<0.001. **B)** Relationship between the wild-type replication program, the checkpoint regulation of origin firing, and genome instability during replication stress. The Spearman's correlation coefficients (ρ) are indicated. ***: p-value<0.001. Top: The profile of average origin efficiencies in wild-type cells as in Fig. 1C (black, left y-axis) is displayed together with the sum of the changes in origin usage as in A (*rad3Δ* - WT, red, right y-axis). x-axis: chromosome coordinates. These two parameters show a strong negative correlation. Bottom: A strong negative correlation is also observed between the replication program (black, left y-axis) and the density of Rad52 (blue, right y-axis, as in A) along the chromosomes. x-axis: chromosome coordinates.

Figure 5: Modulation of the replication program results in redistribution of deregulated origins. A) Profiles of replication efficiency domains in *cdc25-22* (WT, black, as in Fig. 1C) and *cdc25-22 rif1Δ* (*rif1Δ*, blue) cells. Cells were arrested in G2 and released to undergo S phase in 6 mM HU. The averages of origin

efficiencies in each background were assessed for continuous 1000-probe windows. Horizontal lines: average origin efficiency genome-wide. x-axis: chromosome coordinates, y-axes: average origin efficiencies. The full maps of origin usage are shown in Supplemental Fig. S5B. **B)** Origin efficiencies in a representative region of the genome for *rif1Δ* (black) and *rif1Δ rad3Δ* (green) cells synchronized in G2 using the *cdc25-22* mutation and released into 6 mM HU. Asterisks: *rif1*-CIOs. Full efficiency maps are in Supplemental Fig. S5C. x-axis: chromosome coordinates, y-axis: origin efficiencies. **C)** Comparison of the distribution of deregulated origins: *rif1*-CIOs (*rif1Δ rad3Δ*, green bars) vs. CIOs (*rad3Δ*, red bars). x-axis: chromosome coordinates.

Figure 6: Alteration of the replication program results in genome-wide changes in Rad52 accumulation. A-D) *rif1Δ* and *rif1Δ rad3Δ* cells were synchronized using *cdc25-22* and released in 6 mM HU except where indicated. **A)** Rad52 binding and origin usage in a representative region of the genome. Top: profiles of Rad52 recruitment in *rif1Δ* (gray) and *rif1Δ rad3Δ* (orange). The full Rad52 profiles are in Supplemental Fig. S6D, top panel. y-axis: Rad52 binding (IP/input). Bottom: origin efficiencies for *rif1Δ* (black) and *rif1Δ rad3Δ* (green). Asterisks mark *rif1*-CIOs. y-axis: origin efficiency. The full origin efficiency profiles are in Supplemental Fig. S5C. x-axis for top and bottom: chromosome coordinates. **B)** Heat maps of Rad52 binding centered on origins in *rif1Δ* and *rif1Δ rad3Δ* cells treated with 6 mM HU (left, +HU) or in the absence of HU (right, -HU). Presentation is as in Fig. 3B. Note that as in Fig. 3B, there are a few red horizontal lines in *rif1Δ rad3Δ* in –HU: these represent high levels of Rad52 recruitment to the end of the right arm of chromosome III (Supplemental Fig. S6D), which we have not further investigated in this study. **C)** Correlation between changes in origin usage and in Rad52 binding between *rif1Δ rad3Δ* and *rif1Δ* cells. Analysis is as in Fig. 3D. x-axis: difference in origin efficiency, y-axis: difference in Rad52 binding. **D)** Density of Rad52 sites in *rif1Δ rad3Δ* (purple) vs. *rad3Δ* (blue, as in Fig. 4A) calculated over continuous 1000-probe windows. Top panel: +HU, bottom panel: -HU. x-axis: chromosome coordinates, y-axes: density of Rad52 sites.

References

Aguilera A, García-Muse T. 2013. Causes of genome instability. *Annu Rev Genet* **47**: 1–32.

Ahuja AK, Jodkowska K, Teloni F, Bizard AH, Zellweger R, Herrador R, Ortega S, Hickson ID, Altmeyer M, Méndez J, et al. 2016. A short G1 phase imposes constitutive replication stress and fork remodelling in mouse embryonic stem cells. *Nature Communications* **7**: 10660.

Ait Saada A, Teixeira-Silva A, Iraqui I, Costes A, Hardy J, Paoletti G, Fréon K, Lambert SAE. 2017. Unprotected Replication Forks Are Converted into Mitotic Sister Chromatid Bridges. *Mol Cell* **66**: 398–410.e4.

Alvino GM, Collingwood D, Murphy JM, Delrow J, Brewer BJ, Raghuraman MK. 2007. Replication in hydroxyurea: it's a matter of time. *Mol Cell Biol* **27**: 6396–6406.

Bähler J, Wu JQ, Longtine MS, Shah NG, McKenzie A, Steever AB, Wach A, Philippsen P, Pringle JR. 1998. Heterologous modules for efficient and versatile PCR-based gene targeting in Schizosaccharomyces pombe. *Yeast* **14**: 943–951.

Benson FE, Baumann P, West SC. 1998. Synergistic actions of Rad51 and Rad52 in recombination and DNA repair. *Nature* **391**: 401–404.

Bester AC, Roniger M, Oren YS, Im MM, Sarni D, Chaoat M, Bensimon A, Zamir G, Shewach DS, Kerem B. 2011. Nucleotide deficiency promotes genomic instability in early stages of cancer development. *Cell* **145**: 435–446.

Brown EJ, Baltimore D. 2000. ATR disruption leads to chromosomal fragmentation and early embryonic lethality. *Genes Dev* **14**: 397–402.

Chen C-L, Rappailles A, Duquenne L, Huvet M, Guilbaud G, Farinelli L, Audit B, d'Aubenton-Carafa Y, Arneodo A, Hyrien O, et al. 2010. Impact of replication timing on non-CpG and CpG substitution rates in mammalian genomes. *Genome Research* **20**: 447–457.

Cornacchia D, Dileep V, Quivy J-P, Foti R, Tili F, Santarella-Mellwig R, Antony C, Almouzni G, Gilbert DM, Buonomo SBC. 2012. Mouse Rif1 is a key regulator of the replication-timing programme in mammalian cells. *EMBO J* **31**: 3678–3690.

Czajkowsky DM, Liu J, Hamlin JL, Shao Z. 2008. DNA combing reveals intrinsic temporal disorder in the replication of yeast chromosome VI. *Journal of Molecular Biology* **375**: 12–19.

Daigaku Y, Keszthelyi A, Müller CA, Miyabe I, Brooks T, Retkute R, Hubank M, Nieduszynski CA, Carr AM. 2015. A global profile of replicative polymerase usage. *Nat Struct Mol Biol* **22**: 192–198.

Di Rienzi SC, Collingwood D, Raghuraman MK, Brewer BJ. 2009. Fragile genomic sites are associated with origins of replication. *Genome Biology and Evolution* **1**: 350–363.

Dimitrova DS, Gilbert DM. 2000. Temporally coordinated assembly and disassembly of replication factories in the absence of DNA synthesis. *Nat Cell Biol* **2**: 686–694.

Donley N, Thayer MJ. 2013. DNA replication timing, genome stability and cancer: late and/or delayed DNA replication timing is associated with increased genomic instability. *Semin Cancer Biol* **23**: 80–89.

Eykelenboom JK, Harte EC, Canavan L, Pastor-Peidro A, Calvo-Asensio I, Llorens-Agost M, Lowndes NF. 2013. ATR activates the S-M checkpoint during unperturbed growth to ensure sufficient replication prior to mitotic onset. *CellReports* **5**: 1095–1107.

Feng W, Collingwood D, Boeck ME, Fox LA, Alvino GM, Fangman WL, Raghuraman MK, Brewer BJ. 2006. Genomic mapping of single-stranded DNA in hydroxyurea-challenged yeasts identifies origins of replication. *Nat Cell Biol* **8**: 148–155.

Feng W, Di Rienzi SC, Raghuraman MK, Brewer BJ. 2011. Replication stress-induced chromosome breakage is correlated with replication fork progression and is preceded by single-stranded DNA formation. *G3 (Bethesda)* **1**: 327–335.

Forsburg SL, Rhind N. 2006. Basic methods for fission yeast. *Yeast* **23**: 173–183.

Foti R, Gnan S, Cornacchia D, Dileep V, Bulut-Karslioglu A, Diehl S, Buness A, Klein FA, Huber W, Johnstone E, et al. 2016. Nuclear Architecture Organized by Rif1 Underpins the Replication-Timing Program. *Mol Cell* **61**: 260–273.

Fragkos M, Ganier O, Coulombe P, Méchali M. 2015. DNA replication origin activation in space and time. *Nat Rev Mol Cell Biol* **16**: 360–374.

Ge XQ, Blow JJ. 2010. Chk1 inhibits replication factory activation but allows dormant origin firing in existing factories. *J Cell Biol* **191**: 1285–1297.

Gordon JL, Byrne KP, Wolfe KH. 2009. Additions, losses, and rearrangements on the evolutionary route from a reconstructed ancestor to the modern Saccharomyces cerevisiae genome. *PLoS Genet* **5**: e1000485.

Gregan J, Lindner K, Brimage L, Franklin R, Namdar M, Hart EA, Aves SJ, Kearsey SE. 2003. Fission yeast Cdc23/Mcm10 functions after pre-replicative complex formation to promote Cdc45 chromatin binding. *Mol Biol Cell* **14**: 3876–3887.

Guarino E, Salguero I, Kearsey SE. 2014. Cellular regulation of ribonucleotide reductase in eukaryotes. *Semin Cell Dev Biol* **30**: 97–103.

Halazonetis TD, Gorgoulis VG, Bartek J. 2008. An oncogene-induced DNA damage model for cancer development. *Science* **319**: 1352–1355.

Hayano M, Kanoh Y, Matsumoto S, Renard-Guillet C, Shirahige K, Masai H. 2012. Rif1 is a global regulator of timing of replication origin firing in fission yeast. *Genes Dev* **26**: 137–150.

Hayashi M, Katou Y, Itoh T, Tazumi A, Tazumi M, Yamada Y, Takahashi T, Nakagawa T, Shirahige K, Masukata H. 2007. Genome-wide localization of pre-RC sites and identification of replication origins in fission yeast. *EMBO J* **26**: 1327–1339.

Hayles J, Nurse P. 1992. Genetics of the fission yeast Schizosaccharomyces pombe. *Annu Rev Genet* **26**: 373–402.

Heichinger C, Penkett CJ, Bähler J, Nurse P. 2006. Genome-wide characterization of fission yeast DNA replication origins. *EMBO J* **25**: 5171–5179.

Hiraoka Y, Toda T, Yanagida M. 1984. The NDA3 gene of fission yeast encodes beta-tubulin: a cold-sensitive nda3 mutation reversibly blocks spindle formation and chromosome movement in mitosis. *Cell* **39**: 349–358.

Hiratani I, Ryba T, Itoh M, Rathjen J, Kulik M, Papp B, Fussner E, Bazett-Jones DP, Plath K, Dalton S, et al. 2010. Genome-wide dynamics of replication timing revealed by in vitro models of mouse embryogenesis. *Genome Research* **20**: 155–169.

Hiratani I, Ryba T, Itoh M, Yokochi T, Schwaiger M, Chang C-W, Lyou Y, Townes TM, Schübeler D, Gilbert DM. 2008. Global reorganization of replication domains during embryonic stem cell differentiation. *PLoS Biol* **6**: e245.

Hoffman CS, Winston F. 1987. A ten-minute DNA preparation from yeast efficiently releases autonomous plasmids for transformation of Escherichia coli. *Gene* **57**: 267–272.

Hoffman EA, McCulley A, Haarer B, Arnak R, Feng W. 2015. Break-seq reveals hydroxyurea-induced chromosome fragility as a result of unscheduled conflict between DNA replication and transcription. *Genome Research* **25**: 402–412.

Karnani N, Dutta A. 2011. The effect of the intra-S-phase checkpoint on origins of replication in human cells. *Genes Dev* **25**: 621–633.

Kaykov A, Nurse P. 2015. The spatial and temporal organization of origin firing during the S-phase of fission yeast. *Genome Research* **25**: 391–401.

Koren A, Polak P, Nemesh J, Michaelson JJ, Sebat J, Sunyaev SR, McCarroll SA. 2012. Differential relationship of DNA replication timing to different forms of human mutation and variation. *Am J Hum Genet* **91**: 1033–1040.

Labib K, De Piccoli G. 2011. Surviving chromosome replication: the many roles of the S-phase checkpoint pathway. *Philosophical Transactions of the Royal Society B: Biological Sciences* **366**: 3554–3561.

Lam MH, Liu Q, Elledge SJ, Rosen JM. 2004. Chk1 is haploinsufficient for multiple functions critical to tumor suppression. *Cancer Cell* **6**: 45–59.

Lambert S, Mizuno K, Blaisonneau J, Martineau S, Chanet R, Fréon K, Murray JM, Carr AM, Baldacci G. 2010. Homologous recombination restarts blocked replication forks at the expense of genome rearrangements by template exchange. *Mol Cell* **39**: 346–359.

Lang GI, Murray AW. 2011. Mutation rates across budding yeast chromosome VI are correlated with replication timing. *Genome Biology and Evolution* **3**: 799–811.

Lisby M, Rothstein R, Mortensen UH. 2001. Rad52 forms DNA repair and recombination centers during S phase. *Proc Natl Acad Sci USA* **98**: 8276–8282.

Liu L, De S, Michor F. 2013. DNA replication timing and higher-order nuclear organization determine single-nucleotide substitution patterns in cancer genomes. *Nature Communications* **4**: 1502.

Lopez-Mosqueda J, Maas NL, Jonsson ZO, Defazio-Eli LG, Wohlschlegel J, Toczyski DP. 2010. Damage-induced phosphorylation of Sld3 is important to block late origin firing. *Nature* **467**: 479–483.

Mantiero D, Mackenzie A, Donaldson A, Zegerman P. 2011. Limiting replication initiation factors execute the temporal programme of origin firing in budding yeast. *EMBO J* **30**: 4805–4814.

McCune HJ, Danielson LS, Alvino GM, Collingwood D, Delrow JJ, Fangman WL, Brewer BJ, Raghuraman MK. 2008. The temporal program of chromosome replication: genomewide replication in clb5{Delta} Saccharomyces cerevisiae. *Genetics* **180**: 1833–1847.

Mickle KL, Ramanathan S, Rosebrock A, Oliva A, Chaudari A, Yompakdee C, Scott D, Leatherwood J, Huberman JA. 2007. Checkpoint independence of most DNA replication origins in fission yeast. *BMC Mol Biol* **8**: 112.

Moreno S, Klar A, Nurse P. 1991. Molecular genetic analysis of fission yeast Schizosaccharomyces pombe. *Meth Enzymol* **194**: 795–823.

Muller CA, Nieduszynski CA. 2012. Conservation of replication timing reveals global and local regulation of replication origin activity. *Genome Research* **22**: 1953–1962.

Patel PK, Arcangioli B, Baker SP, Bensimon A, Rhind N. 2006. DNA replication origins fire stochastically in fission yeast. *Mol Biol Cell* **17**: 308–316.

Poli J, Tsaponina O, Crabbé L, Keszthelyi A, Pantesco V, Chabes A, Lengronne A, Pasero P. 2012. dNTP pools determine fork progression and origin usage under replication stress. *EMBO J* **31**: 883–894.

Rhind N, Gilbert DM. 2013. DNA replication timing. *Cold Spring Harbor Perspectives in Biology* **5**: a010132.

Rivera-Mulia JC, Buckley Q, Sasaki T, Zimmerman J, Didier RA, Nazor K, Loring JF, Lian Z, Weissman S, Robins AJ, et al. 2015. Dynamic changes in replication timing and gene expression during lineage specification of human pluripotent stem cells. *Genome Research* **25**: 1091–1103.

Rivera-Mulia JC, Gilbert DM. 2016. Replicating Large Genomes: Divide and Conquer. *Mol Cell* **62**: 756–765.

RStudio Team (2015). RStudio: Integrated Development for R. RStudio, Inc., Boston, MA. URL: http://www.rstudio.com.

Ryba T, Hiratani I, Lu J, Itoh M, Kulik M, Zhang J, Schulz TC, Robins AJ, Dalton S, Gilbert DM. 2010. Evolutionarily conserved replication timing profiles predict long-range chromatin interactions and distinguish closely related cell types. *Genome Research* **20**: 761–770.

Santocanale C, Diffley JF. 1998. A Mec1- and Rad53-dependent checkpoint controls late-firing origins of DNA replication. *Nature* **395**: 615–618.

Shechter D, Costanzo V, Gautier J. 2004. ATR and ATM regulate the timing of DNA replication origin firing. *Nat Cell Biol* **6**: 648–655.

Shirahige K, Hori Y, Shiraishi K, Yamashita M, Takahashi K, Obuse C, Tsurimoto T, Yoshikawa H. 1998. Regulation of DNA-replication origins during cell-cycle progression. *Nature* **395**: 618–621.

Stamatoyannopoulos JA, Adzhubei I, Thurman RE, Kryukov GV, Mirkin SM, Sunyaev SR. 2009. Human mutation rate associated with DNA replication timing. *Nat Genet* **41**: 393–395.

Syljuåsen RG, Sørensen CS, Hansen LT, Fugger K, Lundin C, Johansson F, Helleday T, Sehested M, Lukas J, Bartek J. 2005. Inhibition of human Chk1 causes increased initiation of DNA replication, phosphorylation of ATR targets, and DNA breakage. *Mol Cell Biol* **25**: 3553–3562.

Symington LS. 2002. Role of RAD52 epistasis group genes in homologous recombination and double-strand break repair. *Microbiol Mol Biol Rev* **66**: 630–70– table of contents.

Tanaka T, Umemori T, Endo S, Muramatsu S, Kanemaki M, Kamimura Y, Obuse C, Araki H. 2011. Sld7, an Sld3-associated protein required for efficient chromosomal DNA replication in budding yeast. *EMBO J* **30**: 2019–2030.

Taricani L, Wang TSF. 2006. Rad4TopBP1, a scaffold protein, plays separate roles in DNA damage and replication checkpoints and DNA replication. *Mol Biol Cell* **17**: 3456–3468.

Toledo LI, Altmeyer M, Rask M-B, Lukas C, Larsen DH, Povlsen LK, Bekker-Jensen S, Mailand N, Bartek J, Lukas J. 2013. ATR prohibits replication catastrophe by preventing global exhaustion of RPA. *Cell* **155**: 1088–1103.

van Bakel H, van Werven FJ, Radonjic M, Brok MO, van Leenen D, Holstege FCP, Timmers HTM. 2008. Improved genome-wide localization by ChIP-chip using double-round T7 RNA polymerase-based amplification. *Nucleic Acids Research* **36**: e21.

Van Dyck E, Stasiak AZ, Stasiak A, West SC. 1999. Binding of double-strand breaks in DNA by human Rad52 protein. *Nature* **398**: 728–731.

Wold MS. 1997. Replication protein A: a heterotrimeric, single-stranded DNA-binding protein required for eukaryotic DNA metabolism. *Annu Rev Biochem* **66**: 61–92.

Wu P-YJ, Nurse P. 2009. Establishing the program of origin firing during S phase in fission Yeast. *Cell* **136**: 852–864.

Wu P-YJ, Nurse P. 2014. Replication origin selection regulates the distribution of meiotic recombination. *Mol Cell* **53**: 655–662.

Yamazaki S, Ishii A, Kanoh Y, Oda M, Nishito Y, Masai H. 2012. Rif1 regulates the replication timing domains on the human genome. *EMBO J* **31**: 3667–3677.

Zegerman P, Diffley JFX. 2010. Checkpoint-dependent inhibition of DNA replication initiation by Sld3 and Dbf4 phosphorylation. *Nature* **467**: 474–478.

Zeman MK, Cimprich KA. 2014. Causes and consequences of replication stress. *Nat Cell Biol* **16**: 2–9.

Zhou Z-X, Zhang M-J, Peng X, Takayama Y, Xu X-Y, Huang L-Z, Du L-L. 2013. Mapping genomic hotspots of DNA damage by a single-strand-DNA-compatible and strand-specific ChIP-seq method. *Genome Research* **23**: 705–715.

Figure 1

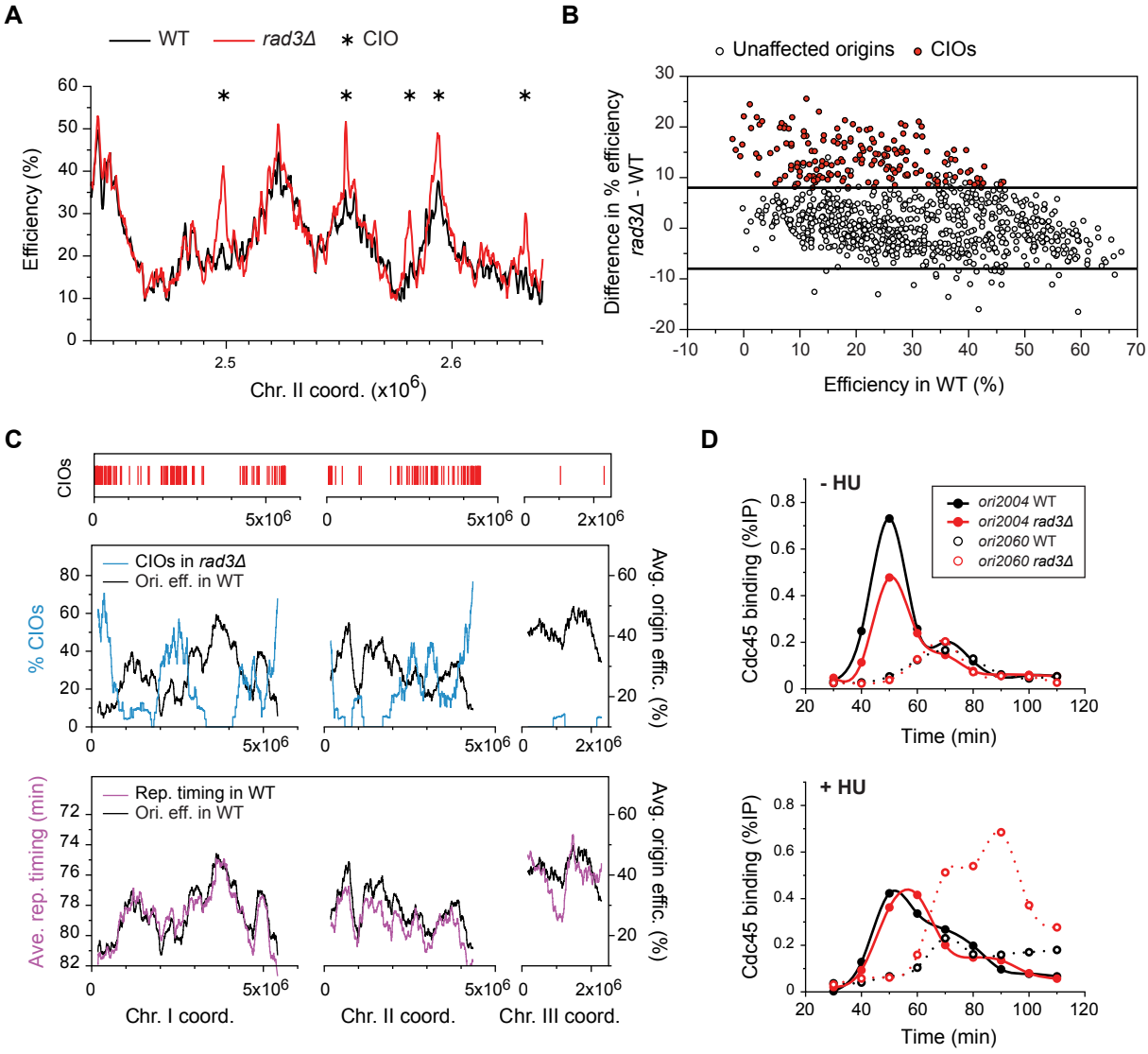

Figure 2

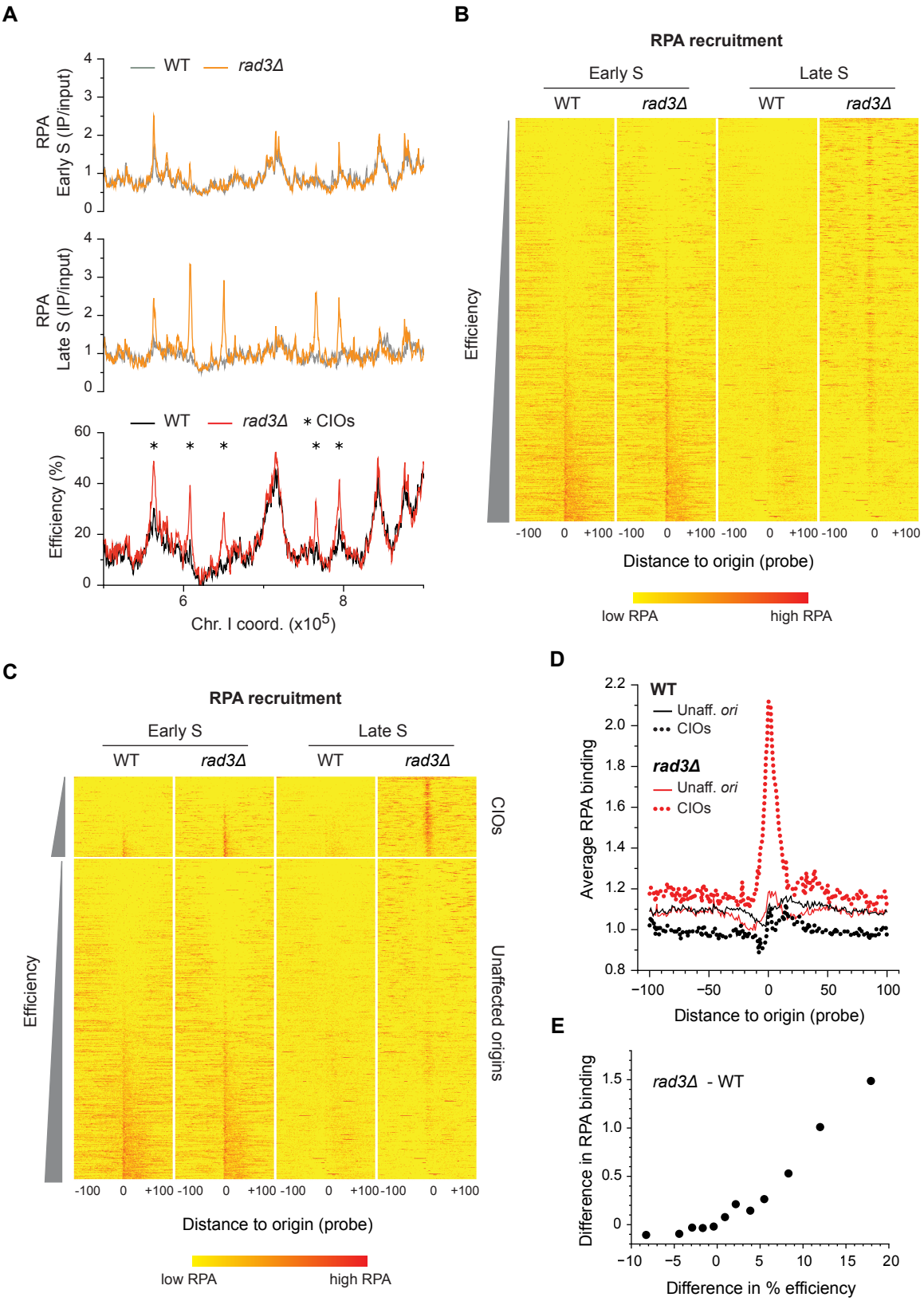

Figure 3

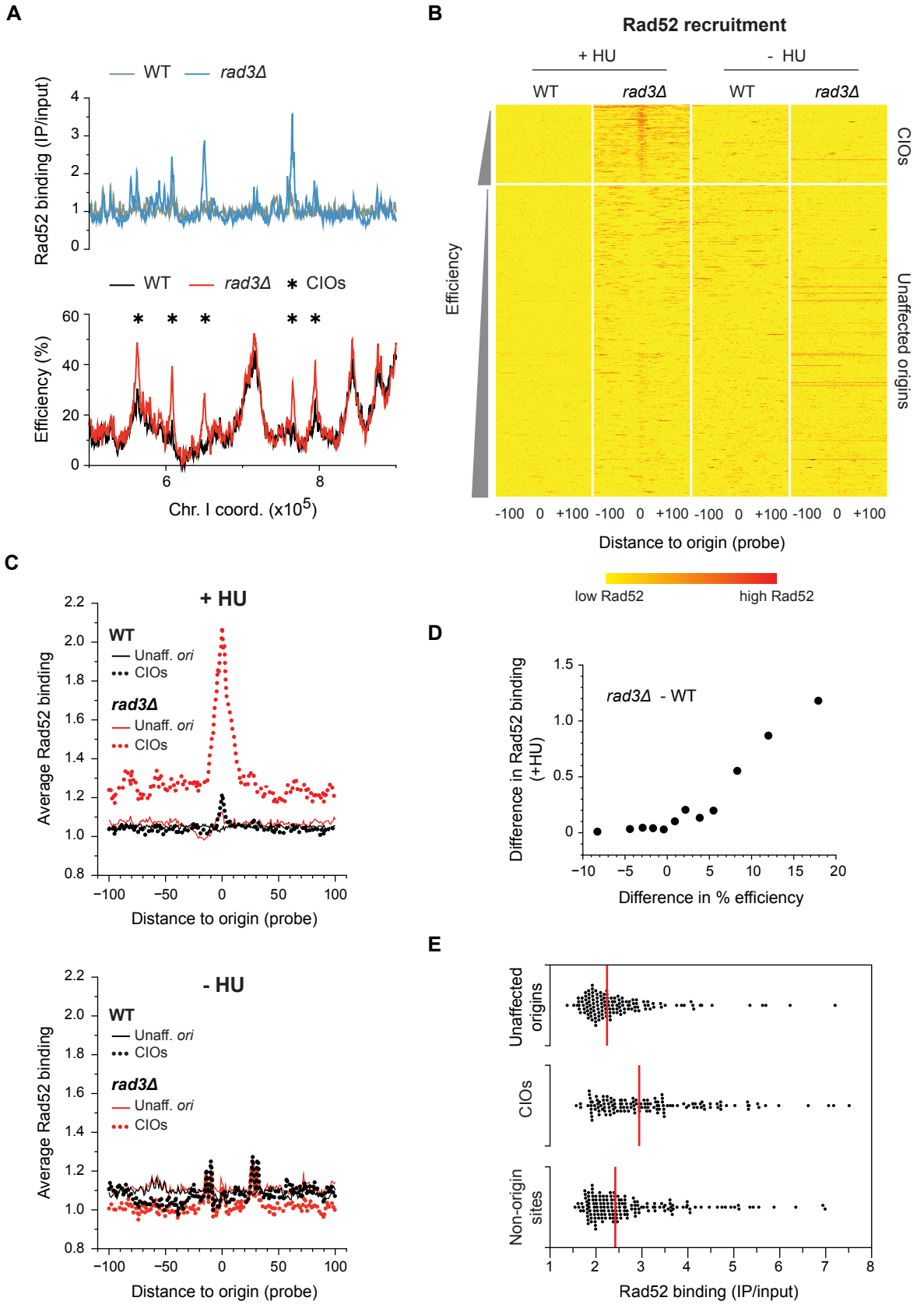

Figure 4

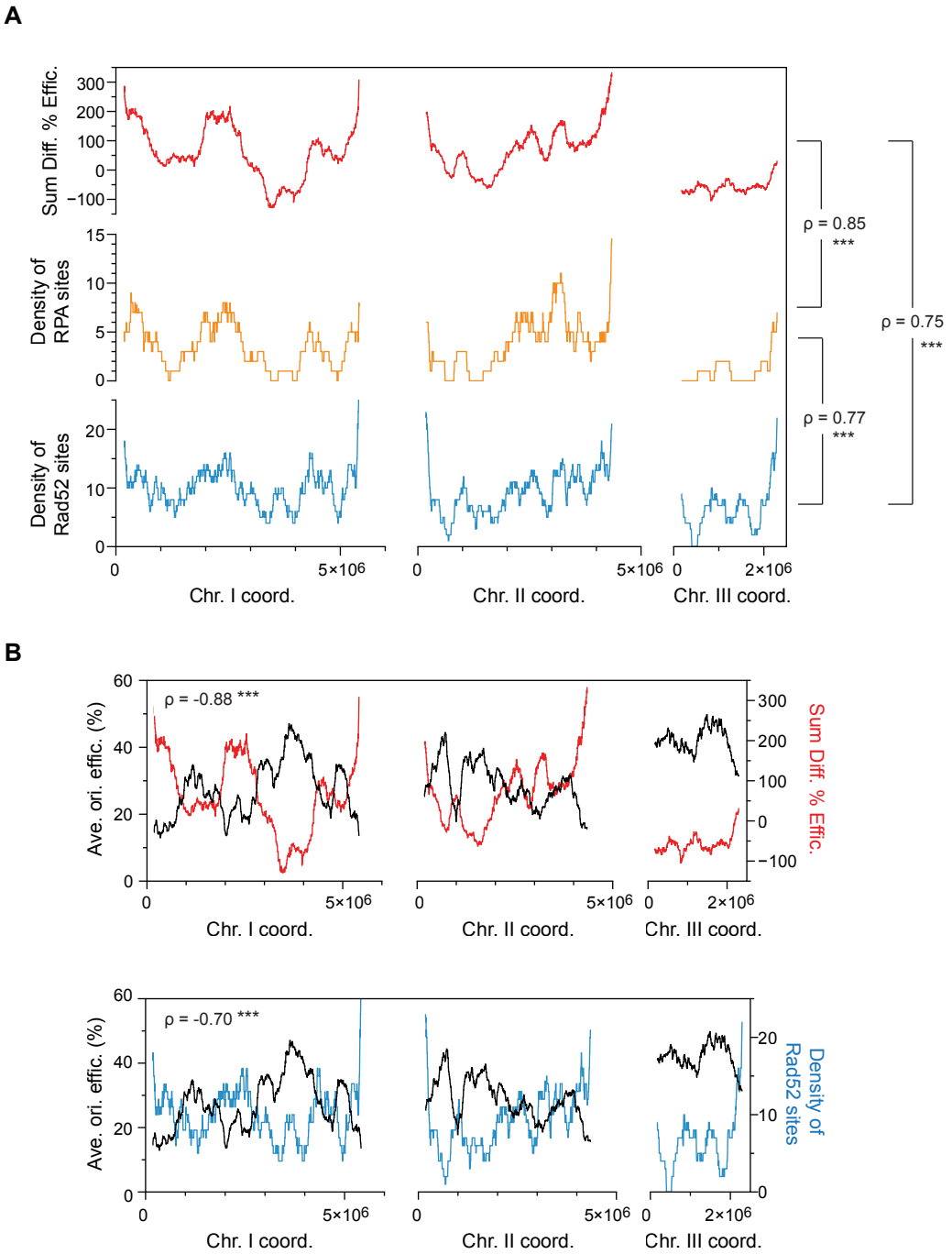

Figure 5

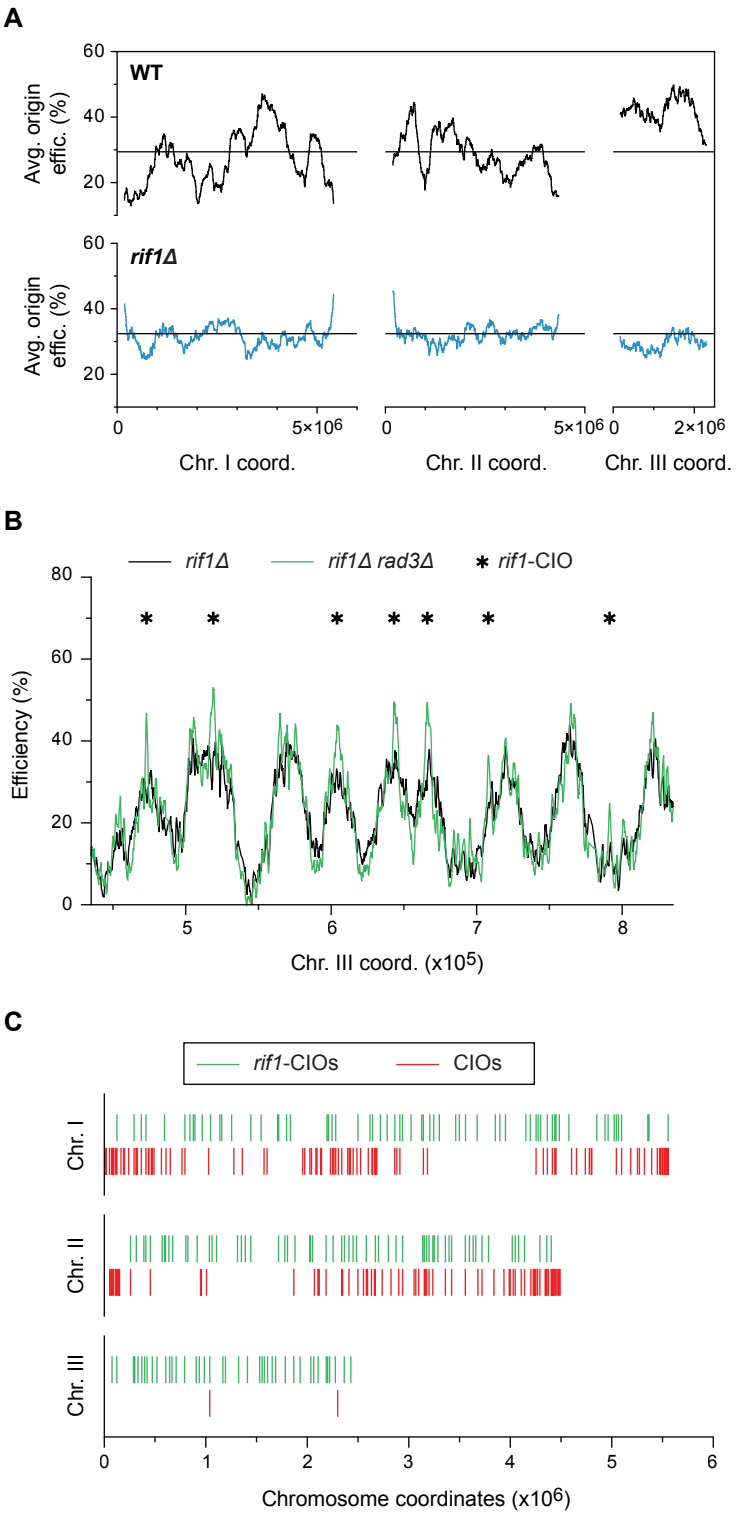

Figure 6